Ceramics International 48 (2022) 19818–19823

Contents lists available at ScienceDirect

Ceramics International

journal homepage: www.elsevier.com/locate/ceramint

Anti-coking and anti-carburizing behavior of amorphous $AlPO_4$ coating

F.S. Sayyedan *, M.H. Enayati, S.M. Nahvi, M. Taghipour

Department of Materials Engineering, Isfahan University of Technology, Isfahan, 8415683111, Iran

ARTICLE INFO

Keywords:
$AlPO_4$
Amorphous
Coating
Anti-coking
Anti-carburizing

ABSTRACT

The aim of the present study was to examine the anti-coking and anti-carburizing behavior of amorphous $AlPO_4$ coating. So, aluminum phosphate composition was synthesized by sol-gel process and applied on the AISI 304 stainless steel by dip coating technique. Anti-coking performance was examined in a tube furnace at 1000 °C for 30 min under Ethane (C_2H_6) atmosphere. Carburizing test was performed in a sealed charcoal medium at 1100 °C for a total of 30 h exposure time. Phase composition of the samples was analyzed by X-Ray Diffraction (XRD) after coking and carburizing tests. Scanning Electron Microscopy (SEM) and Energy Dispersive X-Ray Spectroscopy (EDS) were employed to study the morphology and elemental analysis of the samples after coke and carbon formation experiments. Microhardness indenter was applied on the cross section of the carbon-exposed specimens to plot the hardness profile through the carburizing zone. The results of the coking experiment revealed catalytic coke formed on the uncoated surface, while irregular spherical coke with no trace of catalytic coke was formed on the coated surface, indicating the great anti-coking performance of the amorphous $AlPO_4$ coating. The results of pack-carburizing test demonstrated that the thickness of the carbide layer formed on the bare surface was ~10 times greater than that of the coated sample. Hardness measurement for the amorphous $AlPO_4$ coated sample detected lower values compared to those for the uncoated one at all distances from the surface, indicating less carbon diffusion occurred beneath the coated surface. In overall, the results declared that the amorphous $AlPO_4$ coating could be a good candidate for surface protection of stainless steel against catalytic coke formation and carbon diffusion.

1. Introduction

Thermal cracking of hydrocarbons is classified as one of the most important industrial processes in which Olefins (C_nH_{2n}) including Ethylene (C_2H_4) and Propylene (C_3H_6) would be formed as desirable products [1]. However, coke build up on the inner wall of the tubes is inevitable and causes some detrimental effects including reduction of heat transfer, restriction of the flow of the hydrocarbon feedstock, and increase in the fuel consumption [2]. The outcome would be the consequent shutdown for decoking operation followed by decrease in expected service lifetime. Therefore, coke formation could be a serious problem in the combustion chamber of gas turbines and thermal cracking furnaces in petrochemical industries [2,3]. In general, coking and carburization are considered as the two main corrosion issues in hydrocarbon cracking in reformer tubes of the petrochemical plants [4].

Some methods have been employed to prevent coke formation during the past few years, such as choosing the right alloy in the manufacturing process of the tubes, using sulfide inhibitors, and applying protective coatings on the inner wall of the cracking tubes [5].

Applying the right coating on the inner wall of the pyrolysis furnaces can dramatically moderate the destructive phenomenon of catalytic coke formation [6,7]. In this regard, Li and Yang [4] used a glass-based coating containing SiO_2, BaO, CaO, and Al_2O_3 oxides to control the carburizing phenomenon. Their results showed that the uncoated HP steel was heavily carburized, as plenty of catalytic coke was formed on its surface after the coking test. On the contrary, the glass coating prevented severe carburization and catalytic coke formation. In addition, Tang et al. [8] investigated the anti-coking behavior of TiC, TiN, and TiO_2 coatings applied by chemical vapor deposition (CVD). Although all three coatings presented suitable performance, the anti-coking behavior of the TiN and TiC coatings was found superior than that of the TiO_2 coating. Bao et al. [9] used the $MnCr_2O_4$ spinel coating deposited by selective oxidizing. They achieved satisfactory results of anti-coking performance during light naphtha thermal cracking. Indeed, the spinel coating prevented the formation of catalytic coke. In another study, Tang et al. [10] investigated the anti-coking properties of TiN coatings

* Corresponding author.
E-mail address: fs.sayyedan@alumni.iut.ac.ir (F.S. Sayyedan).

https://doi.org/10.1016/j.ceramint.2022.03.256
Received 5 November 2021; Received in revised form 18 March 2022; Accepted 25 March 2022
Available online 28 March 2022

applied at different deposition temperatures. Coatings applied at temperatures below 850 °C did not show acceptable anti-coking behavior due to the presence of microcracks, while the coatings applied at temperatures above 850 °C presented excellent anti-coking performance. Zhang et al. [11] studied the anti-coking behavior of TiO_2 coating applied by metal organic chemical vapor deposition (MOCVD) method. It was shown that time and temperature of the coating process significantly affected the morphology of the coatings. The best anti-coking performance was attributed to the crack-free coating applied at 250 °C for 80 min. Taghipour et al. [12] used gas-phased aluminide coatings to improve the anti-coking efficiency of the HP-MA steel. They showed that the aluminide coatings had better anti-coking performance compared to the HP-MA steel. Moreover, it was specified that the higher the Al content in the coating, the better the anti-coking performance.

Amorphous aluminum phosphate ($AlPO_4$) with chemically inert nature and non-crystalline structure can be considered as a suitable protective coating material for a broad range of applications involved in corrosion issues. Amorphous $AlPO_4$ acts as a durable diffusion barrier layer against destructive species, and so presents promising anti-carburizing and anti-coking property due to the lack of grain boundaries and other crystalline defects [13]. Moreover, it can be used as a high temperature engineering ceramic material without volume changes and subsequent stresses caused by the polymorphic transformations (berlinite, tridymite, and cristobalite) concerning with the crystalline aluminum phosphate [14].

The oxidation behavior of amorphous aluminum phosphate coating was studied in our previous work [15]. The objective of the present research was to study of the anti-coking and anti-carburizing behavior of the sol-gel derived amorphous $AlPO_4$ coating. Preventing coke buildup and carbon deposition on the inner wall of the pyrolysis furnaces were the main purposes of the current research.

2. Materials and methods

2.1. Substrate pretreatment

Chemical composition of the AISI 304 stainless steel substrate is presented in Table 1 according to the optical emission spectroscopy (OES) (Metal Scan Arun 2500, England) analysis. The sheet with thickness of 1 mm was cut in to 20 × 20 mm^2 coupons using a spark wire machine. The samples were grounded using 800, 1200, and 2400 grit SiC papers and polished by 0.1 μm alumina slurry. The specimens were degreased ultrasonically in acetone and deionized water for 20 min, respectively.

2.2. Coating preparation

Amorphous $AlPO_4$ composition was synthesized by sol-gel process. Aluminum nitrate nonahydrate ($Al(NO_3)_3{\cdot}9H_2O$, Merck, 98.5% purity) and phosphorus pentoxide (P_2O_5, Merck, 98% purity) were dissolved in ethanol (C_2H_5OH, Merck, 99.8% purity) to reach Al/P:1.75/1 M ratio. The two solutions were mixed together and stirred for 1 h. 5 wt % Polyvinylpyrrolidone ($(C_6H_9NO)_n$, Sigma-Aldrich) was dissolved to the above solution. Stainless steel coupons were dip coated into the resulting solution for 1 min with a constant withdrawal rate of 20 mm/min. The coated samples were dried at 150 °C and annealed at 500 °C for 1 h to eliminate all organic compounds and get a uniform coating with chemical bonding to the substrate.

2.3. Coating characterization

2.3.1. Coking test

Anti-coking performance of the coated and uncoated substrates was investigated in a tube furnace. The specimens were laid on the ceramic boats and then put into the quartz tube reactor. Ethane (C_2H_6) was considered as the input hydrocarbon feedstock and cracking was performed at 1000 °C for 30 min. It is worth noting that samples were heated in argon in order to remove oxygen from the reactor. After the furnace reached a temperature of 1000 °C, ethane was replaced with argon to start the cracking process. The inlet ethane flow rate was adjusted to 0.6 L/h. After completing the coking test, the reactor was cleaned by argon for 15 min to remove the gas products obtained during the cracking process. The anti-coking ratio (η) was calculated at the end of the coking test as follows [11]:

$$\eta = [(M_2 - M_1) / M_2] \times 100\% \quad (1)$$

Where, M_1 and M_2 are the mass of the coke deposited on the coated and uncoated surfaces after the coking test, respectively.

2.3.2. Carburizing test

Both coated and uncoated specimens were packed into an alumina crucible stuffed with charcoal and sealed with a high temperature glue. The set was heated up to 1100 °C and kept in this temperature for 30 h, then cooled down to room temperature.

2.3.3. Phase composition and morphology observations

Phase composition analysis of the coated and uncoated samples before and after carburizing test was performed by an X-ray diffractometer (XRD, Philips Xpert) using Ni filtered Cu Kα radiation (λ = 0.154 nm, 40 kV, 30 mA) over the 2θ range of 10°–90°.

The surface and cross-sectional morphologies of the coated and uncoated samples before and after coking and carburizing tests were observed by scanning electron microscope (SEM, Philips XL30) equipped with an energy-dispersive spectroscopy (EDS). Glow discharge optical emission spectrometry (GDOES, GDA 750 HR) technique operated at 700 V and regulated pressure of 2.3 hPa was performed to assess the composition and thickness of the coating.

2.3.4. Microhardness measurement

Vickers microhardness measurement was performed at a load of 100 g and dwell time of 10 s to evaluate the hardness changes through the carburizing zone. The coated and uncoated carburized samples were cross-cut, mounted, grounded to 2400 grit SiC paper, and polished by 0.1 μm alumina slurry. Microhardness indenter was applied on each sample in three different lines from surface to the bulk to plot the hardness profile through the carburizing zone.

3. Results and discussion

3.1. Coating characterization

The XRD patterns of the as-synthesized powder after drying and annealing steps are presented in Fig. 1. It is clearly seen that the as-synthesized $AlPO_4$ composition shows no crystalline features. There is only a broad hump at 2θs ~20°–30°, indicating the completely amorphous nature of the synthesized coating material, which is based on a synthetic aluminum phosphate in which the molar content of aluminum is greater than phosphorus to create a pseudo amorphous structure.

Table 1
OES analysis of the AISI 304 stainless steel.

Element	Fe	C	Si	S	P	Mn	Ni	Cr	Mo	Cu	Nb	Ti	V
Wt. %	Bal.	0.046	0.295	<0.030	<0.007	1.520	11.300	16.000	<0.050	0.164	0.071	0.015	0.054

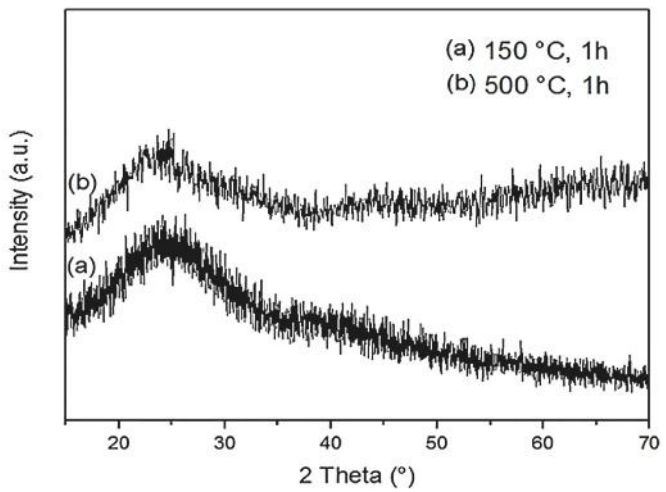

Fig. 1. XRD patterns of the amorphous $AlPO_4$ composition (a) gel dried at 150 °C for 1 h, (b) powder annealed at 500 °C for 1 h.

Fig. 2 exhibits the SEM micrograph and EDS analysis of the applied $AlPO_4$ coating on the surface of the AISI 304 stainless steel. As seen in the SEM image, the coating is uniform, continuous, and crack-free. EDS analysis confirms the formation of an aluminum phosphate layer on the surface revealed by appearing Al and P elements in the analysis.

Fig. 3 exhibits the cross sectional micrograph and GDOES analysis of the amorphous $AlPO_4$ coating formed on the stainless steel 304 after annealing at 500 °C for 1 h.

GDOES analysis presented in Fig. 3a demonstrates that Al and P elements have a meaningful concentration gradient in the surface region, decaying towards the depth, and that the approximate thickness of the coating layer is around 110 nm, where the Fe, Cr, and Ni contents remain almost constant and Al and P contents reduce significantly. Fig. 3b represents the cross-sectional microstructure of the coating after annealing at 500 °C for 1 h. It can be found that the coating is dense, uniform, and with good adhesion to the substrate. The thickness of the coating is estimated to be 110 nm which is in a good accordance with the GDOES observation.

3.2. Coke formation behavior

Fig. 4 represents the weight of the coke deposited on the bare stainless steel 304 and amorphous $AlPO_4$ coated sample after coking test run at 1000 °C for 30 min. As can be seen in Fig. 4, the bare substrate experiments a much higher weight gain per unit area (~7 times greater) than that of the coated sample, indicating deposition of a large volume of carbon on the uncoated stainless steel surface. Moreover, the anti-coking ratio for amorphous $AlPO_4$ coating was estimated to be ~85% (calculated by Eq. (1)), indicating the acceptable and satisfying anti-coking performance of the coating material.

Fig. 5 represents the SEM images of the uncoated and amorphous $AlPO_4$ coated stainless steel surfaces after coke formation test performed at 1000 °C under Ethane (C_2H_6) atmosphere for a total of 30 min exposure time. As it is seen in the SEM micrograph of the bare substrate (Fig. 5a), catalytic coke was significantly formed on the stainless steel surface. In fact, for the alloys with poor coking resistance, catalytic coke is formed at the early minutes of the cracking process. In order to better understanding of catalytic coke formation phenomenon on the surface of the stainless steel 304, the surface degradation due to the catalytic coke formation has been explained below. In the first stage, physical adsorption of carbon occurs on the surface. In general, the series of possible reactions for thermal cracking of ethane have been proposed as follows [16]:

According to reaction (2), Ethane cracks to Ethene and hydrogen. Then, Ethene decomposes to Methane and carbon according to reaction (3).

$$C_2H_6 \rightarrow C_2H_4 + H_2 \quad (2)$$

$$C_2H_4 \rightarrow C + CH_4 \quad (3)$$

On the other hand, Methane can be decomposed to carbon and hydrogen by the following reaction:

$$CH_4 \rightarrow C + 2H_2,\ \Delta G^\circ = 87399 - 108.74T\ (J.mol^{-1}) \quad (4)$$

It is worth noting that the reaction (4) is thermodynamically feasible at 1000 °C, but with sluggish kinetics at this temperature. The decomposition of methane is a moderately endothermic process, and non-catalytic thermal cracking of methane needs temperatures over 1200 °C to have reasonable kinetics [17,18]. Overall, thermal decomposition of hydrocarbon molecules leads to the production of free atomic carbon, which can deposit on the surface of the sample. According to reports, the activation energy of carbon diffusion in 304 stainless steel is 44.6 kcal/mol and its diffusion coefficient at 1000 °C is 1.45×10^{-7} cm^2 s^{-1}, which is a relatively high value [19]. On the other hand, the pre-formed chromium oxide film on the stainless steel surface does not provide the necessary protection to prevent carbon diffusion at a temperature of 1000 °C and reduction environment. So, the deposited carbon diffuses through the metal and precipitate at the grain boundaries. Afterward, metal crystals would remove from the surface by the outward growth of carbon to form filamentous/catalytic coke [20]. This could be possible for metals which dissolve carbon, namely Fe or Ni.

On the other hand, only some irregular spherical cokes were formed on the coated stainless steel surface (Fig. 5b) with no sign of catalytic coke formation. This type of carbon is only caused by the gas phase reactions deposited on the surface. In fact, the amorphous $AlPO_4$ coating

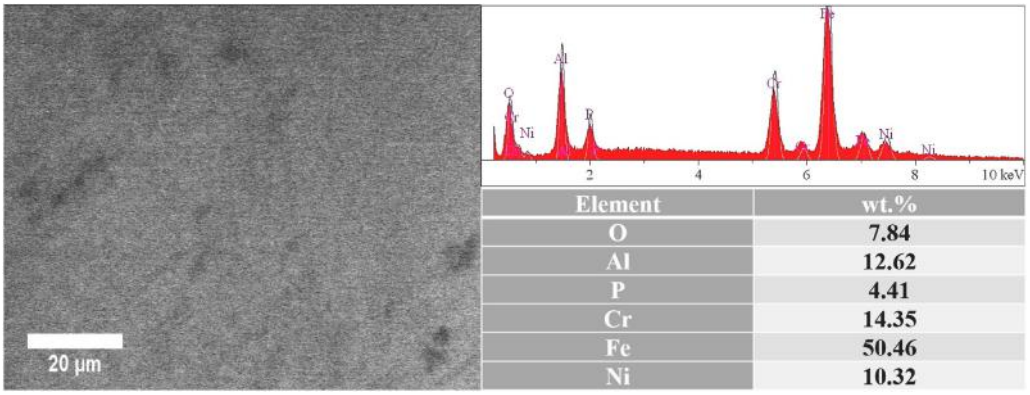

Element	wt.%
O	7.84
Al	12.62
P	4.41
Cr	14.35
Fe	50.46
Ni	10.32

Fig. 2. SEM micrograph and EDS analysis of the $AlPO_4$ coating formed on the stainless steel 304 surface after annealing at 500 °C for 1 h.

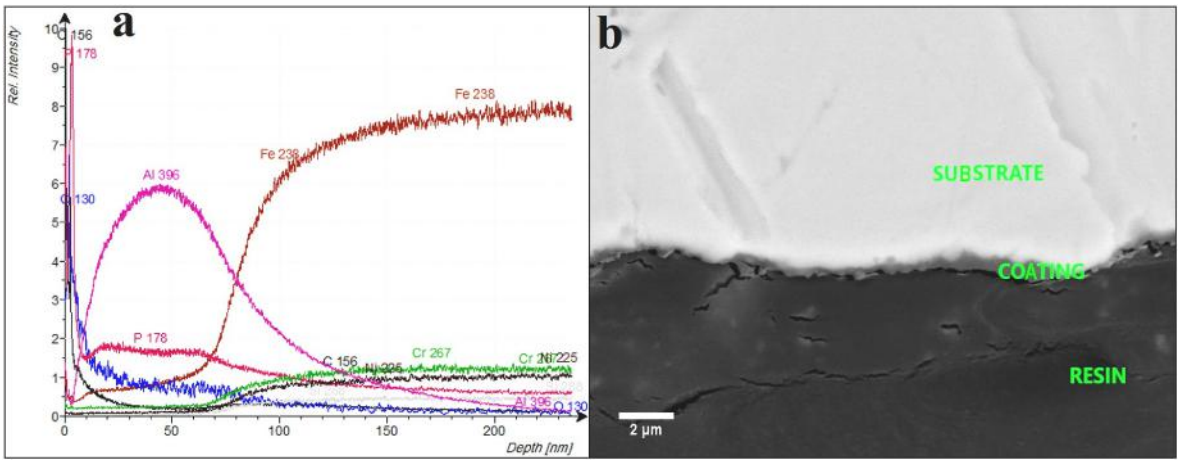

Fig. 3. (a) GDOES analysis and (b) cross-sectional morphology of the amorphous $AlPO_4$ coating after annealing at 500 °C for 1 h.

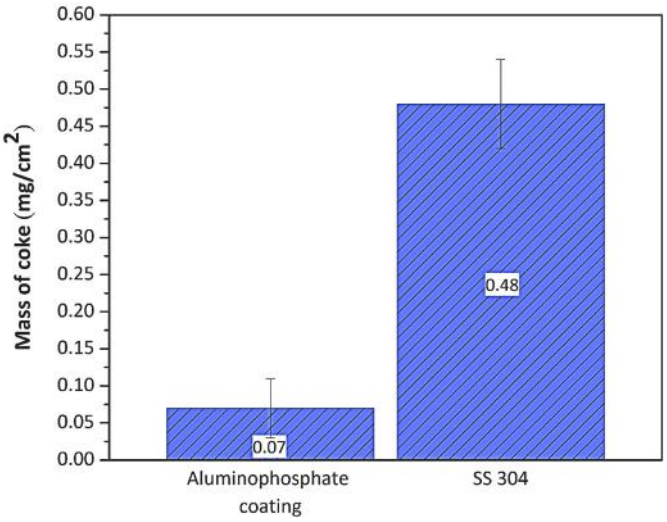

Fig. 4. Weight changes per unit area for AISI 304 stainless steel and amorphous $AlPO_4$ coating after coking test run at 1000 °C for 30 min.

was able to prevent the inward diffusion of carbon and formation of the catalytic coke, indicating the excellent anti-coking performance of the amorphous $AlPO_4$ as a protective coating. This capability is attributed to the amorphous nature of the coating material and its performance as a diffusion barrier in the absence of grain boundaries and other crystalline defects [13]. Since there is excess aluminum content in the precursor solution (Al/P:1.75/1), even in the case that crystallization occurs during long times of cracking at 1000 °C, the amorphous $AlPO_4$ would convert to the crystalline $AlPO_4$ and Al_2O_3 with desirable protection against the inward diffusion of carbon as well as the formation of catalytic coke [21].

3.3. Carburization behavior

Fig. 6 shows the XRD patterns of the uncoated and amorphous $AlPO_4$ coated stainless steel 304 after carburizing test run at 1100 °C for 30 h. The XRD patterns suggest the formation of Cr_7C_3 and Cr_3C_2 carbide phases on the both coated and uncoated specimens. Haider et al. [22] studied the carbon diffusion phenomenon in the 304L austenitic stainless steel at 650–750 °C in 20%–40% CH_4/H_2 atmosphere and reported the formation of the similar carbides on the surface. More details of the formation of these carbides will be explained in the next section.

Fig. 7 represents the SEM cross sectional micrographs of the uncoated and amorphous $AlPO_4$ coated stainless steel 304 after carburizing process at 1100 °C for 30 h. It is observed that the thickness of the carburizing zone in the uncoated and coated specimens is around 20 and 2 µm, respectively, indicating the severe carburization occurred on the bare surface compared to the coated one. According to Fig. 7a, carbide formation is more severe near the surface of the stainless steel. Hence the carbide layer is seen more compact in the lower regions, close to the substrate's surface, as compared to the upper.

Map elemental analysis of the cross-section of the uncoated and amorphous $AlPO_4$ coated samples presented in Fig. 8 offers more clear representation of chemical composition after carburizing test. Accordingly, a layer mostly composed of Cr and C has been developed on the surface of the stainless steel 304, confirming the XRD results presented in Fig. 6. On the other hand, a Cr-depleted zone was found right below

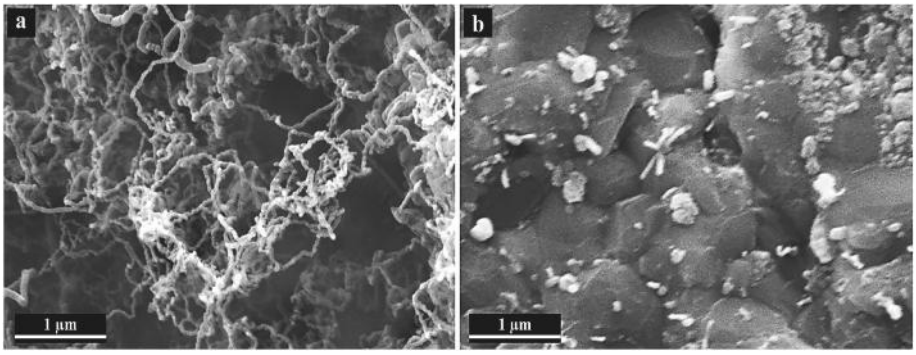

Fig. 5. SEM images of the (a) uncoated and (b) amorphous $AlPO_4$ coated stainless steel 304 surface after coke formation test performed at 1000 °C under Ethane (C_2H_6) atmosphere for a total of 30 min exposure time.

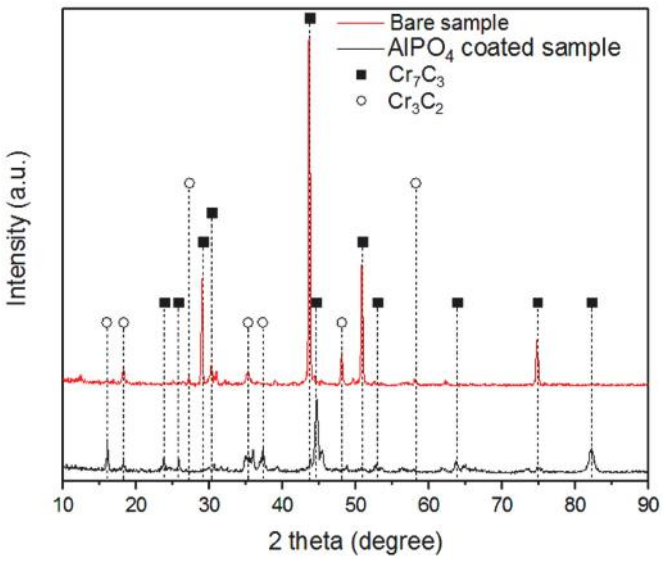

Fig. 6. XRD patterns of the uncoated and amorphous $AlPO_4$ coated stainless steel 304 after carburizing test run at 1100 °C for 30 h.

the carbide layers, where internal oxidation takes place.

In summary, the chromium oxide protective layer on the surface of 304 stainless steel reacts with carbon and converts to non-protective carbides, namely Cr_7C_3 and Cr_3C_2 by reactions (5) and (6) at temperatures above 1100 °C [23]:

$$3\ Cr_2O_3 + 13C = 2\ Cr_3C_2 + 9\ CO \quad (5)$$

$$7\ Cr_2O_3 + 27C = 2\ Cr_7C_3 + 21\ CO \quad (6)$$

Meanwhile, the chromium in the substrate diffuses to the surface to form a relatively protective chromium oxide layer and reacts with the oxygen trapped in the chamber. Then, the chromium oxide layer reacts with the carbon to form non-protective carbides. By repeating this process, the thickness of the carbide layer increases and a chromium-depleted zone is formed near the surface. Due to the loss of chromium, this area is more sensitive to internal oxidation, as shown in Fig. 6.

This scenario is similar for the carburization process of the amorphous $AlPO_4$ coated surface, but with a major difference concerning with the thickness of the carburizing zone which is one tenth of the bare surface (compare Fig. 7a and b). The main role of the amorphous $AlPO_4$ coating is to act as a diffusion barrier against carbon and retard the carbides formation.

Fig. 9 demonstrates the hardness profile across the carburizing zone for the uncoated and amorphous $AlPO_4$ coated stainless steel 304. Accordingly, a descending trend can be observed in the hardness values from the surface to the bulk of the carburized samples. It is clear to be observed that the hardness value is the highest at the samples' surface, where the carbide layer has been formed. This is because of the fact that the carbides are harder than the other phases in the bulk [24]. Furthermore, as seen for the bare sample, the hardness of the carbide layer is higher in the more compact areas than the other regions. On the other hand, the hardness decreases gradually from the surface to the bulk for the both samples. In the areas farther away from the surface, the hardness profile remains almost unchanged and equal the substrate hardness value. By comparing the hardness diagrams, it is clear that the hardness values for the amorphous $AlPO_4$ coated sample are lower than

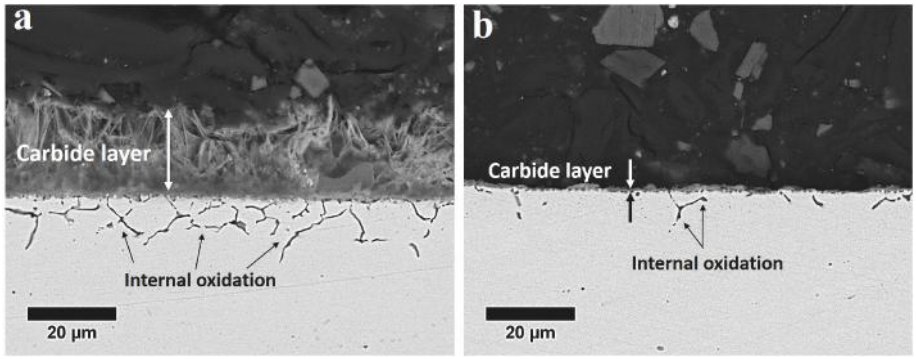

Fig. 7. SEM cross sectional micrographs of (a) uncoated and (b) amorphous $AlPO_4$ coated stainless steel 304 after carburization at 1100 °C for 30 h.

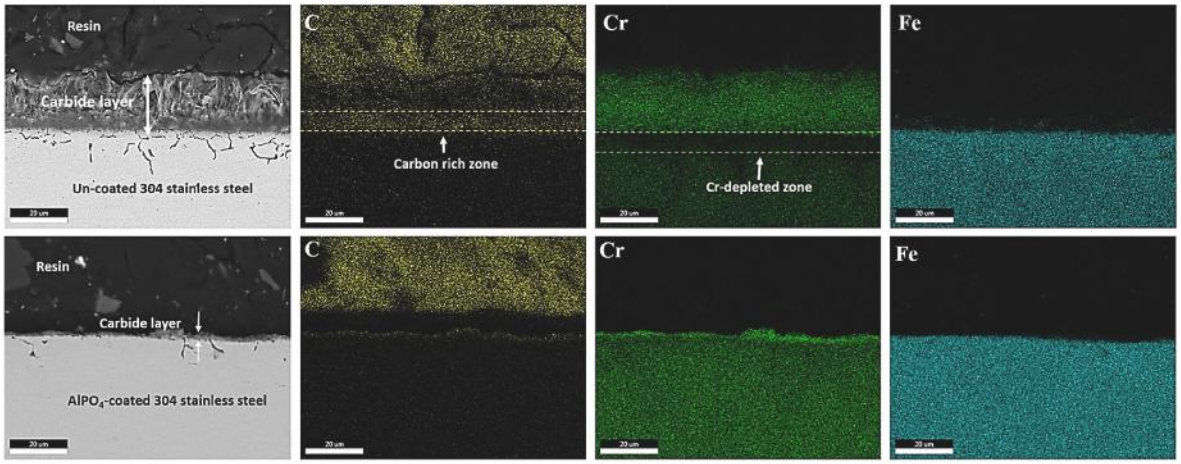

Fig. 8. Map elemental analysis of cross section of the uncoated and amorphous $AlPO_4$ coated stainless steel 304 after carburization at 1100 °C for 30 h.

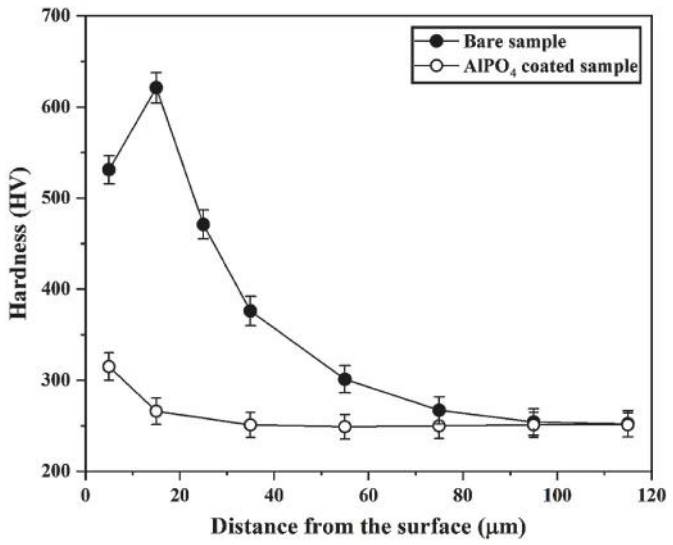

Fig. 9. The hardness distributions of the coated and uncoated specimens from the surface to the bulk after the carburizing test.

those for the uncoated one at all distances from the surface, indicating less carbon diffusion beneath the surface. In conclusion, the amorphous $AlPO_4$ coating acted as a barrier layer against diffusion of carbon during the carburizing test at 1100 °C.

4. Conclusions

An amorphous $AlPO_4$ coating was applied on the AISI 304 stainless steel alloy and anti-coking and anti-carburizing behavior of the coatings were evaluated. The main results were as follows:

1. A large volume of catalytic cokes was formed on the uncoated surface after coking test, while only some irregular spherical cokes were formed on the coated surface and no effects of catalytic coke was observed which revealed the great anti-coking performance of the amorphous $AlPO_4$ coating.
2. The results of pack-carburizing test revealed that the carbon deposited and carbides formed on the coated surface were much less than those on the bare one.
3. The thickness of the carburizing zone for the coated surface was one tenth of the bare one, indicating good ability of the amorphous $AlPO_4$ coating as a diffusion barrier to retard carbon diffusion and carbide formation.
4. The hardness distribution for both the coated and uncoated specimens from the surface to the bulk after the pack-carburizing test revealed higher hardness values where the carbides were presented more compact.
5. The hardness values for the amorphous $AlPO_4$ coated sample were lower than those for the uncoated one at all distances from the surface, indicating less carbon diffusion occurred beneath the coated surface.
6. In overall, the results showed that the amorphous $AlPO_4$ coating was well capable of surface protection of stainless steel alloy against atmospheric attacks including carbon deposition and coke formation.

Declaration of competing interest

The authors declare that they have no known competing financial interests or personal relationships that could have appeared to influence the work reported in this paper.

Acknowledgments

The authors gratefully acknowledge the support of Dr. Abdoulmajid Eslami from Department of Materials Engineering at Isfahan University of Technology to provide required equipment for this research.

References

[1] S.M. Sadrameli, Thermal/catalytic cracking of hydrocarbons for the production of olefins: a state-of-the-art review I: thermal cracking review, Fuel 140 (2015) 102–115.
[2] I. Kucora, P. Paunjoric, J. Tolmac, M. Vulovic, J.G. Speight, L. Radovanovic, Coke formation in pyrolysis furnaces in the petrochemical industry, Petrol. Sci. Technol. 35 (2017) 213–221.
[3] M. Brandauer, A. Schulz, S. Wittig, Mechanisms of coke formation in gas turbine combustion chambers, in: ASME 1995 Int. Gas Turbine Aeroengine Congr. Expo, American Society of Mechanical Engineers, 1995. V003T06A005-V003T06A005.
[4] C.S. Li, Y.S. Yang, A glass based coating for enhancing anti-coking and anti-carburizing abilities of heat-resistant steel HP, Surf. Coating. Technol. 185 (2004) 68–73.
[5] S.H. Symoens, N. Olahova, A.E. Muñoz Gandarillas, H. Karimi, M.R. Djokic, M.-F. Reyniers, G.B. Marin, K.M. Van Geem, State-of-the-art of coke formation during steam cracking: anti-coking surface technologies, Ind. Eng. Chem. Res. 57 (2018) 16117–16136.
[6] C.M. Schietekat, S.A. Sarris, P.A. Reyniers, L.B. Kool, W. Peng, P. Lucas, K.M. Van Geem, G.B. Marin, Catalytic coating for reduced coke formation in steam cracking reactors, Ind. Eng. Chem. Res. 54 (2015) 9525–9535.
[7] A. Ochoa, J. Bilbao, A.G. Gayubo, P. Castaño, Coke formation and deactivation during catalytic reforming of biomass and waste pyrolysis products: a review, Renew. Sustain. Energy Rev. 119 (2020) 109600.
[8] S. Tang, N. Shi, J. Wang, A. Tang, Comparison of the anti-coking performance of CVD TiN, TiO2 and TiC coatings for hydrocarbon fuel pyrolysis, Ceram. Int. 43 (2017) 3818–3823.
[9] B. Bao, Z. Wang, H. Xu, J. Liu, Anti-coking effect of MnCr2O4 spinel coating during light naphtha thermal cracking, Energy Proc. 105 (2017) 4808–4813.
[10] S. Tang, S. Gao, S. Wang, J. Wang, Q. Zhu, Y. Chen, X. Li, Characterization of CVD TiN coating at different deposition temperatures and its application in hydrocarbon pyrolysis, Surf. Coating. Technol. 258 (2014) 1060–1067.
[11] Y. Zhang, S. Zhang, T. Zhang, T. Zou, Q. Zhu, J. Wang, X. Li, Characterization of MOCVD TiO2 coating and its anti-coking application in cyclohexane pyrolysis, Surf. Coating. Technol. 296 (2016) 108–116.
[12] M. Taghipour, A. Eslami, M. Salehi, A. Bahrami, An investigation on anti-coking behavior of gas phase aluminide coatings applied on a high performance micro alloyed (HP-MA) steel, Surf. Coating. Technol. (2020) 125607.
[13] Z.H. Stachurski, On structure and properties of amorphous materials, Materials 4 (2011) 1564–1598.
[14] F.S. Sayyedan, M.H. Enayati, M. Hashempour, A. Vicenzo, M. Bestetti, Synthesis and characterization of sol-gel derived non-stoichiometric aluminum phosphate coating, Surf. Coating. Technol. 351 (2018) 128–135.
[15] F.S. Sayyedan, M.H. Enayati, On structure and oxidation behaviour of non-stoichiometric amorphous aluminium phosphate coating, Surf. Eng. 35 (2019) 670–676.
[16] W. Shen, Y. Wang, X. Shi, N. Shah, F. Huggins, S. Bollineni, M. Seehra, G. Huffman, Catalytic nonoxidative dehydrogenation of ethane over Fe–Ni and Ni catalysts supported on Mg (Al) O to produce hydrogen and easily purified carbon nanotubes, Energy Fuel. 21 (2007) 3520–3529.
[17] H.F. Abbas, W.M.A.W. Daud, Hydrogen production by methane decomposition: a review, Int. J. Hydrogen Energy 35 (2010) 1160–1190.
[18] A. Boretti, A perspective on the production of hydrogen from solar-driven thermal decomposition of methane, Int. J. Hydrogen Energy 46 (2021) 34509–34514.
[19] R.P. Agarwala, M.C. Naik, M.S. Anand, A.R. Paul, Diffusion of carbon in stainless steels, J. Nucl. Mater. 36 (1970) 41–47.
[20] H. Li, Stability of Mn-Cr-O Spinel and Chromium Oxide in High Temerature Ethylene Cracking Environments, 2011.
[21] S. A Sarris, S. H Symoens, N. Olahova, M.-F. Reyniers, G. B Marin, K. M Van Geem, Alumina-based coating for coke reduction in steam crackers, Materials. 13 (2020) 2025.
[22] F.I. Haider, M.H. Suryanto, Carbon Diffusion in 304l Austenitic Stainless Steel at 650-750 O c in Carburizing Environment, (n.d.).
[23] V.K. Simonov, A.M. Grishin, Thermodynamic analysis and the mechanism of the solid-phase reduction of Cr 2 O 3 with carbon: Part 1, Russ. Metall. 2013 (2013) 425–429.
[24] J. Garcia, V.C. Cipres, A. Blomqvist, B. Kaplan, Cemented carbide microstructures: a review, Int. J. Refract. Metals Hard Mater. 80 (2019) 40–68.